Electronic Supplementary Material (ESI) for Nanoscale.
This journal is © The Royal Society of Chemistry 2022

Electronic Supplementary Information

Mosquito-Inspired Design of Resistive Antennae for Ultrasensitive Acoustic Detection

Kaixuan Wang,[a] Shu Gong,[a] Yuxin Zhang,[a] Lim Wei Yap,[a] Wenlong Cheng*[a]

[a]Department of Chemical & Biological Engineering, Monash University, Clayton, Victoria 3800, Australia

*Correspondence author. Email: wenlong.cheng@monash.edu

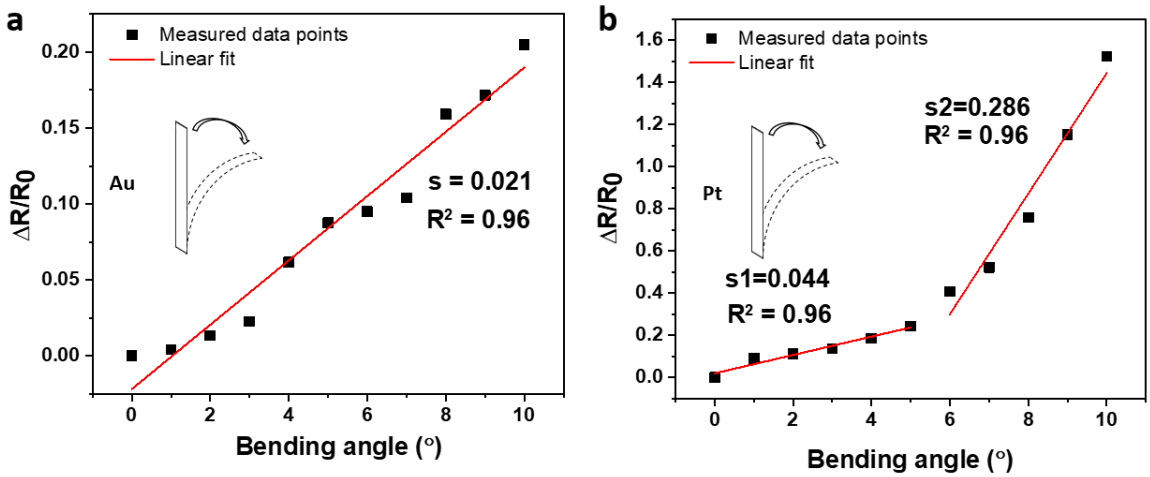

Fig. S1 (a) The resistance change of Au/PDMS strip versus bending angle. The angle increased from 0 to 10° with a step of 1°. We did the linear fitting for the data points. The R^2 value for the fitting is 0.96. The slope of the linear fitting represents the sensor's sensitivity ($\Delta R/R_0$ per angle), which is 0.021. (b) The resistance change of Pt/PDMS strip versus bending angle. The angle increased from 0 to 10° with a step of 1°. We did two linear fittings for the data points. From 0 to 5°, the R^2 value for the fitting is 0.96 and the sensitivity is 0.044; from 6° to 10°, the R^2 value for the fitting is 0.96 and the sensitivity is 0.286.

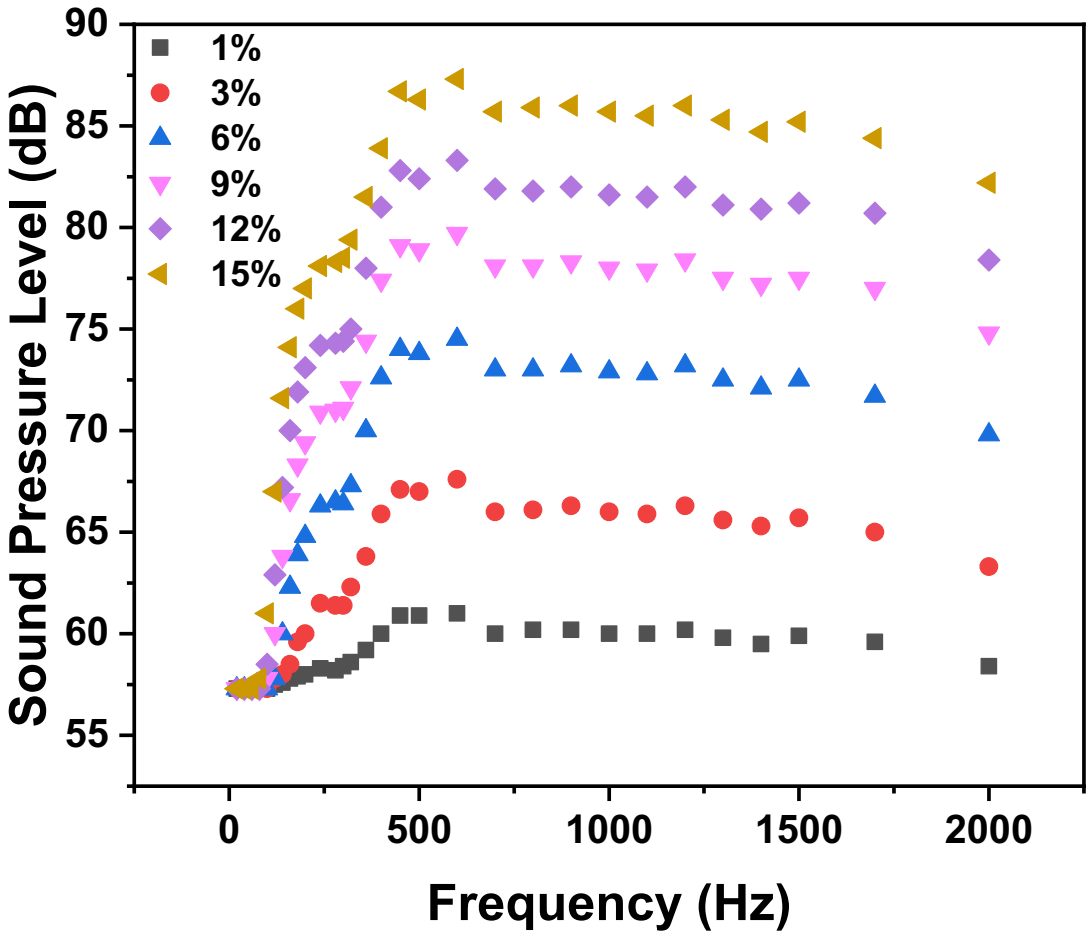

Fig. S2 Sound pressure level versus sound frequency under the sound volume of 1%, 3%, 6%, 9%, 12%, and 15%. The distance between the antennae and speaker is 5 mm.

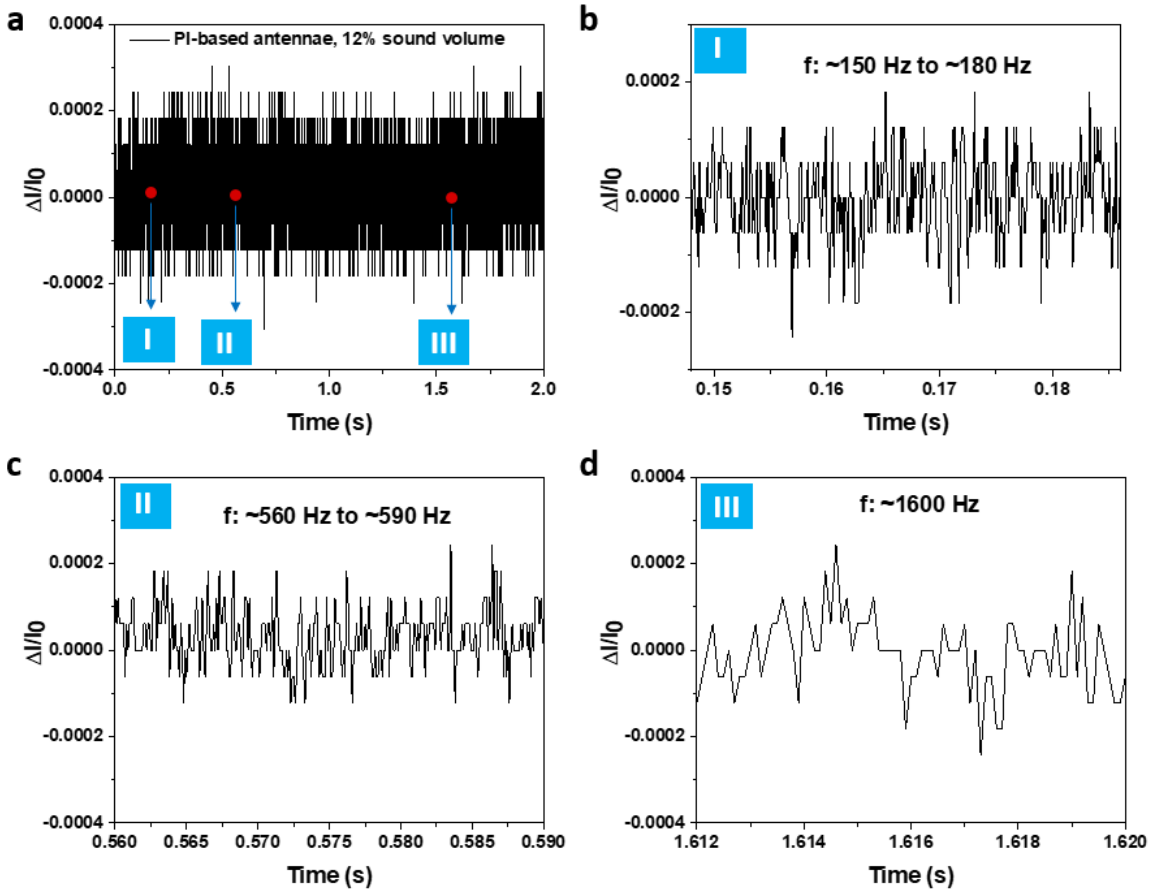

Fig. S3 We used the sound source of 0-2000 Hz with 12% sound volume to stimulate the PI-based antennae (Pt/PI/Pt). (a) Change of output current from the antennae. (b-d) Enlarged view of current changes with time in three different time zones indicated in (a). The antennae could not distinguish the sound frequency.

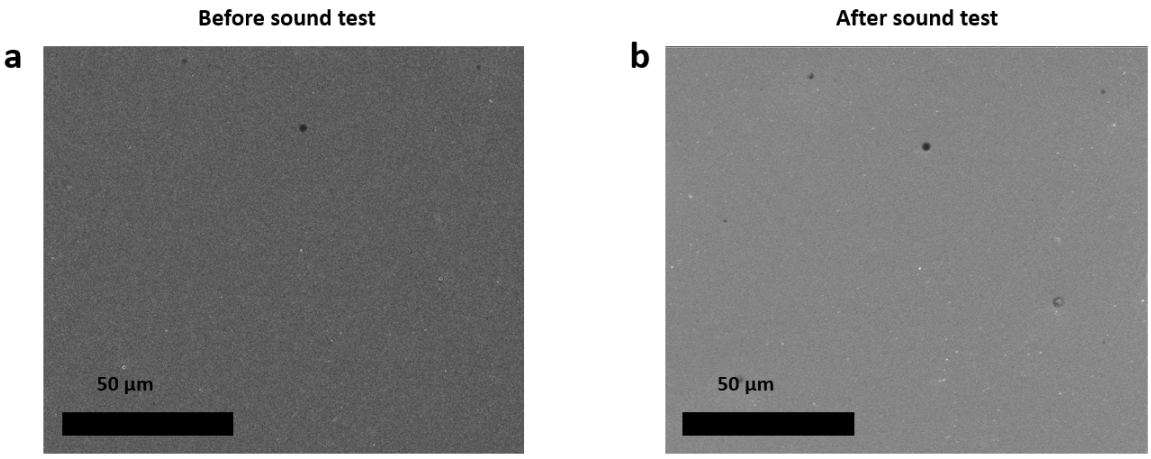

Fig. S4 The "sound test" in above figure means "we used the sound source of 0-2000 Hz with 15% sound volume to stimulate the antennae for 10 times". We observed the Pt film morphology at the middle part of the antennae by SEM characterization. Top-view SEM image of the PI-based antennae (a) before and (b) after the sound test. No change was observed for the film.

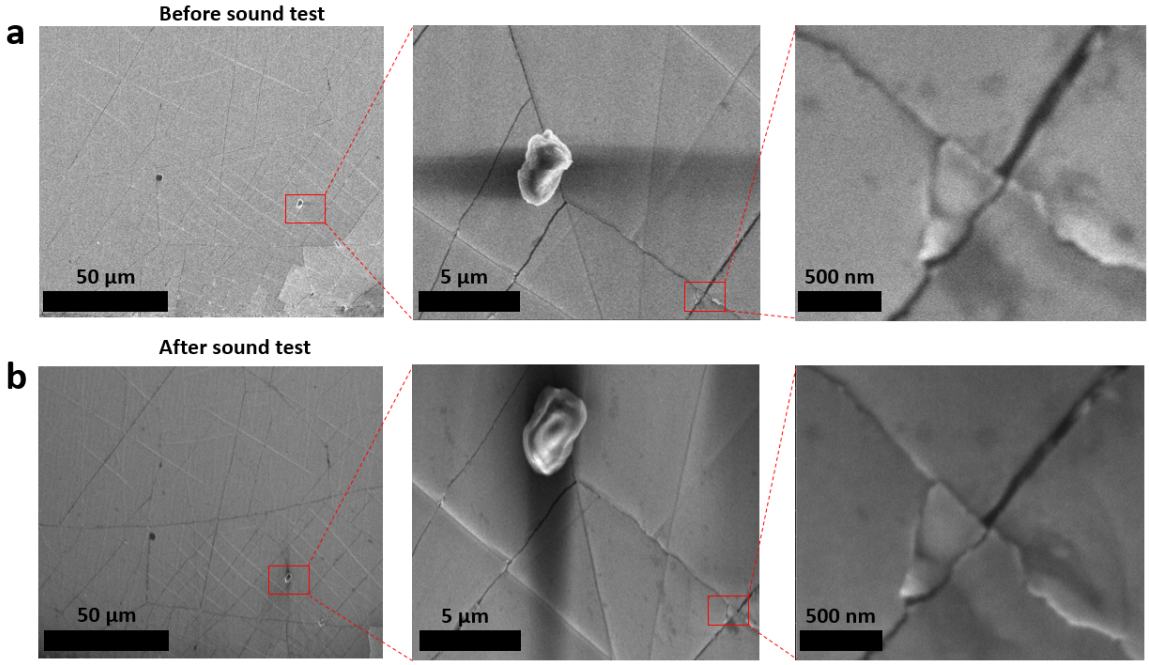

Fig. S5 The "sound test" in above figure means "we used the sound source of 0-2000 Hz with 15% sound volume to stimulate the antennae for 10 times". We observed the Pt film morphology at the middle part of the antennae by SEM characterization. Top-view SEM image of the PDMS-based antennae (a) before and (b) after the sound test. The crack numbers and width did not change after the sound test.

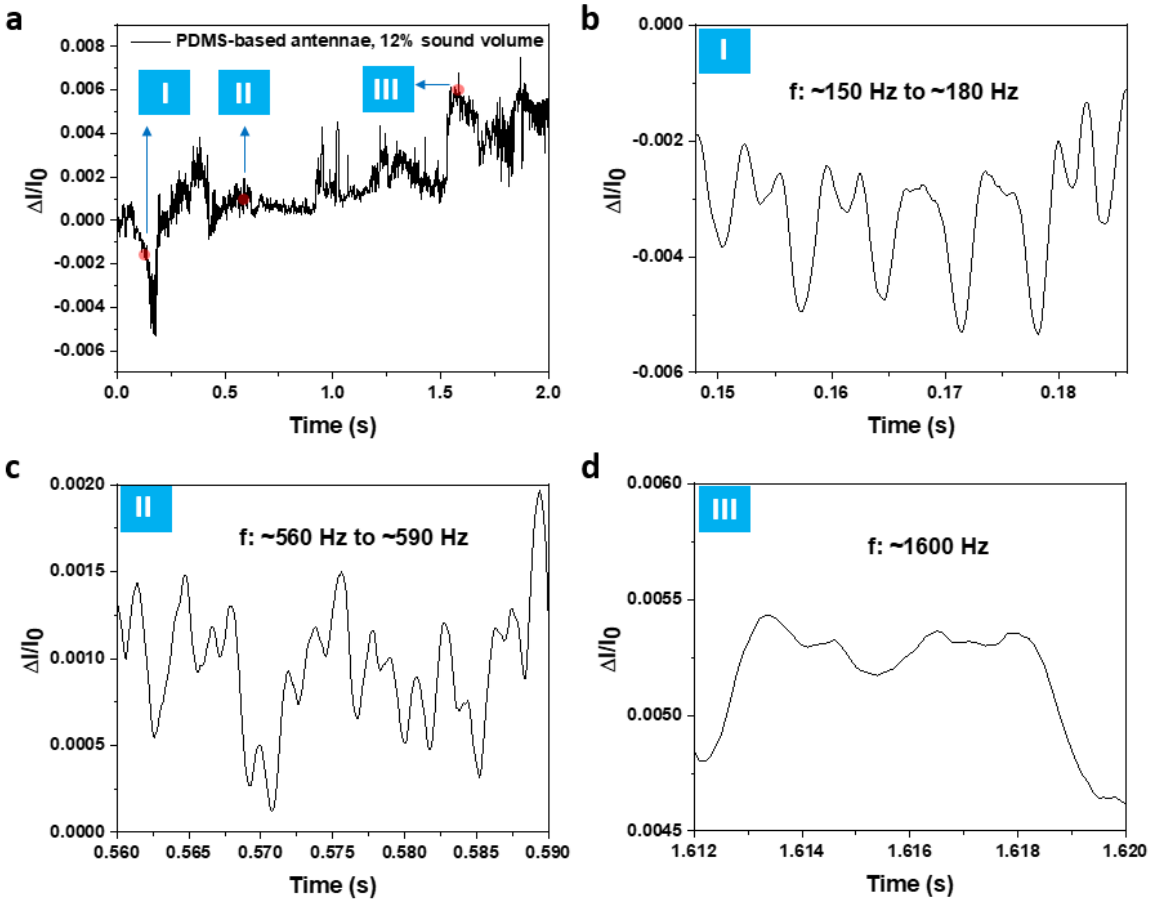

Fig. S6 We used the sound source of 0-2000 Hz with 12% sound volume to stimulate the PDMS-based antennae (Pt/PDMS/Pt). (a) Change of output current from the antennae. (b-d) Enlarged view of current changes with time in three different time zones indicated in (a). The antennae could only distinguish the sound frequency from ~150 Hz to ~590 Hz.

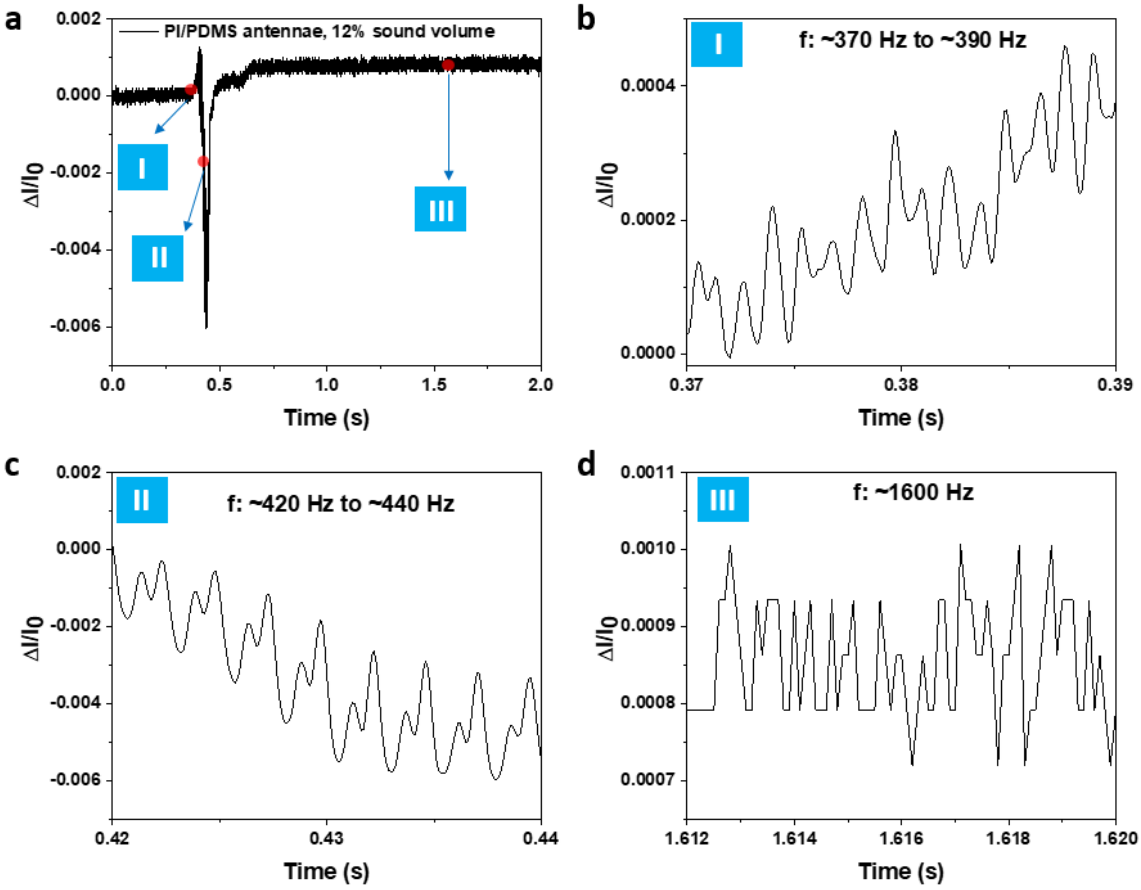

Fig. S7 We used the sound source of 0-2000 Hz with 12% sound volume to stimulate the PI/PDMS-based antennae without joints (Pt/PI/PDMS/Pt). (a) Change of output current from the antennae. (b-d) Enlarged view of current changes with time in three different time zones indicated in (a). The antennae respond to the applied sound from ~370 Hz to ~440 Hz with ~740 Hz to ~880 Hz.

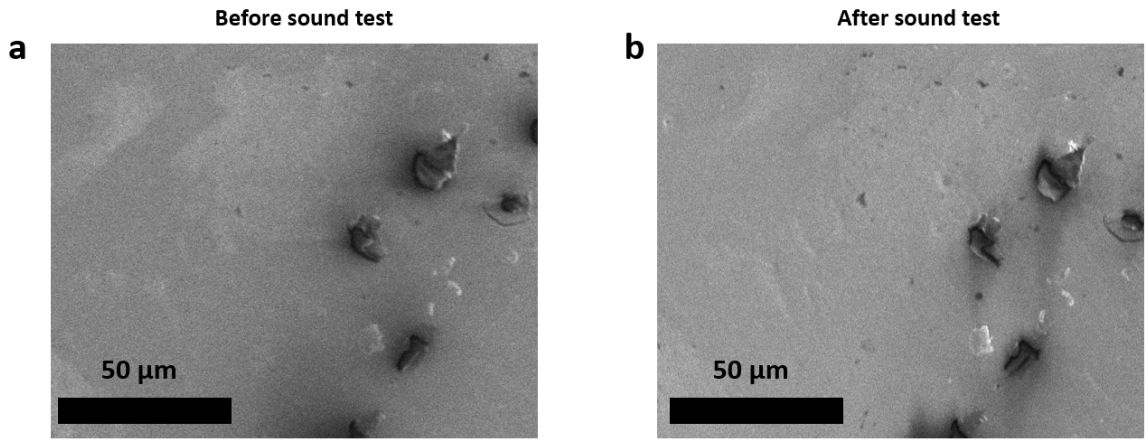

Fig. S8 The "sound test" in above figure means "we used the sound source of 0-2000 Hz with 15% sound volume to stimulate the antennae for 10 times". We observed the Pt film morphology at the middle part of the antennae by SEM characterization. Top-view SEM image of the PI/PDMS-based antennae (a) before and (b) after the sound test. No change was observed for the film.

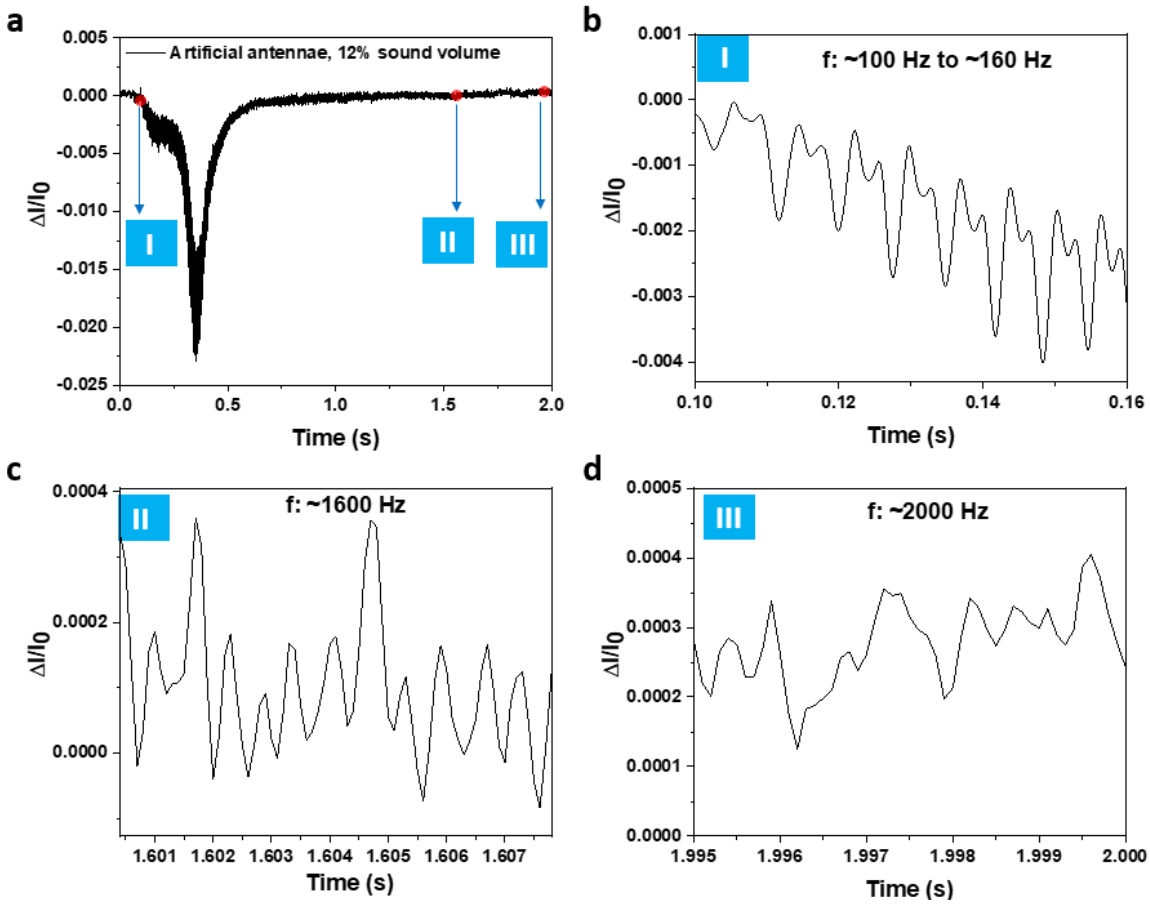

Fig. S9 We used the sound source of 0-2000 Hz with 12% sound volume to stimulate the antennae. (a) Antennae output from the mosquito-inspired artificial antennae. (b-d) Enlarged view of current changes with time in three different time zones indicated in (a). The antennae could distinguish the sound frequency from ~100 Hz to ~1600 Hz.

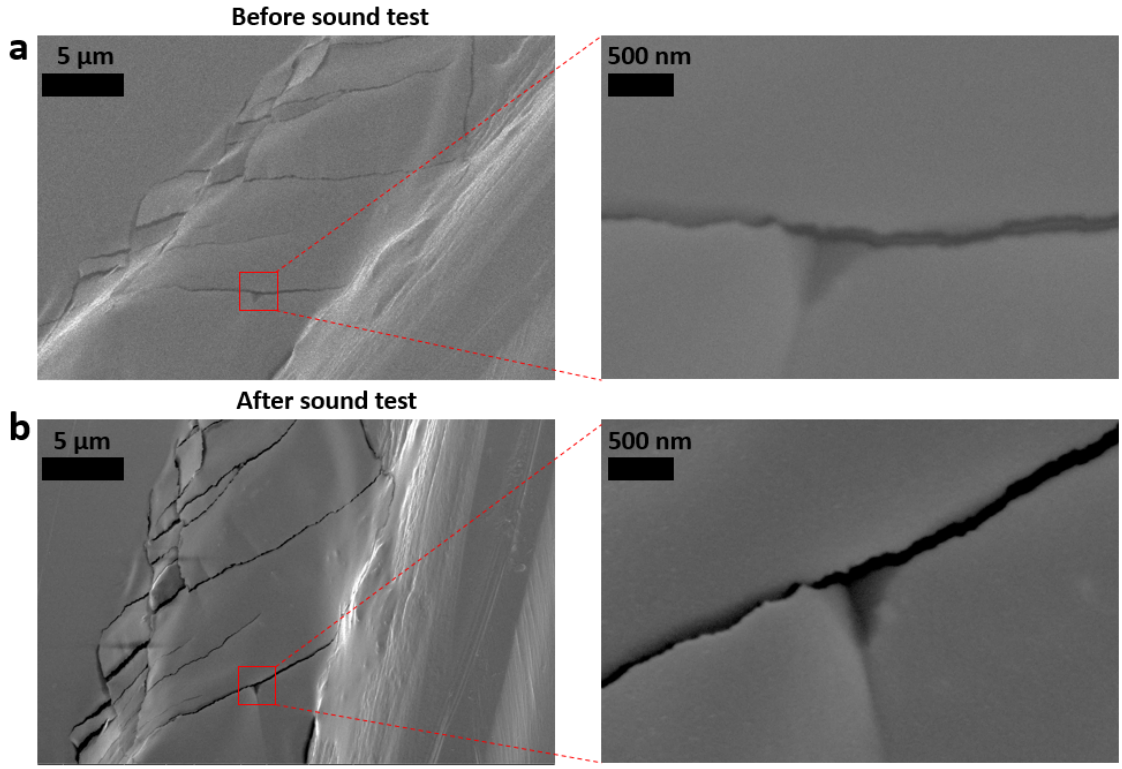

Fig. S10 The "sound test" in above figure means "we used the sound source of 0-2000 Hz with 15% sound volume to stimulate the antennae for 10 times". We observed the Pt film morphology on the soft PDMS joint part of the antennae by SEM characterization. Top-view SEM images of the cracked Pt at PI/PDMS interface and the joint part (a) before and (b) after the sound test. The crack numbers and width did not change after the sound test. We don't show the morphology of Pt film on rigid PI segment part because it is similar to that of Fig. S4.

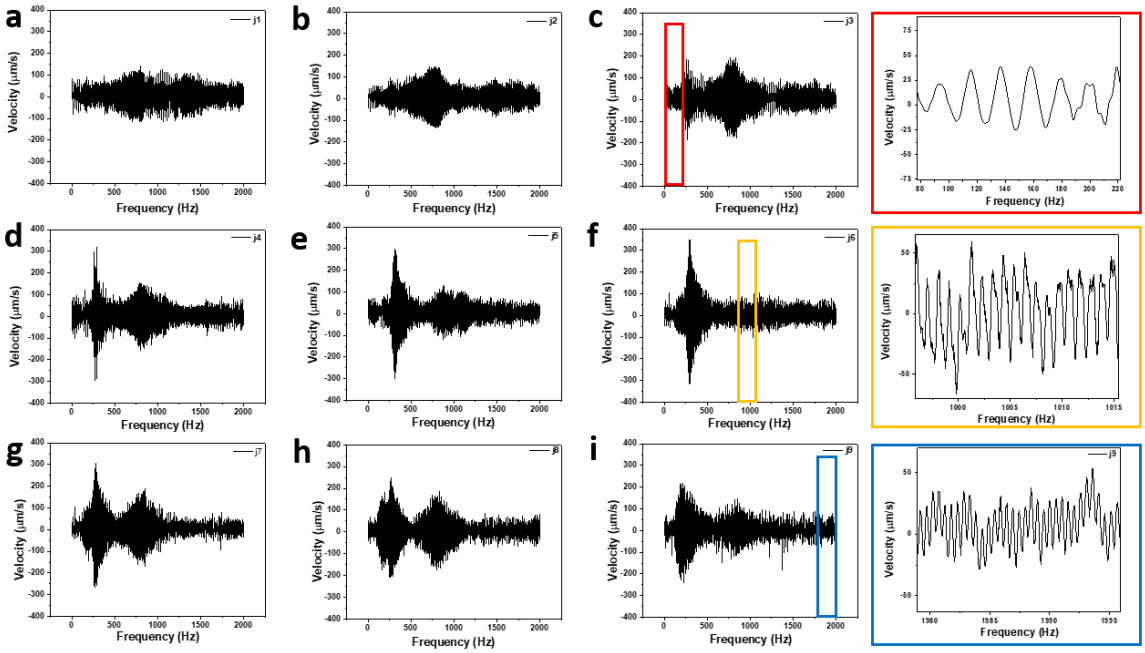

Fig. S11 (a-i) The vibration velocity versus sound frequency from joint-1 to joint-9 of artificial mosquito antennae. The labelling rule for joint's number is that the number increases from 1 to 9 along the antennae.

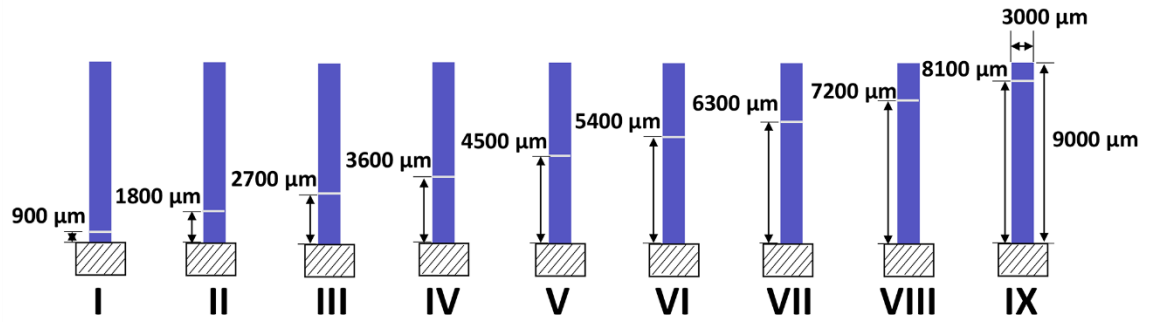

Fig. S12 Dimensions for single-joint antennae. From I to IX, the distance between joint and fixture point kept increasing with a step of 900 µm.

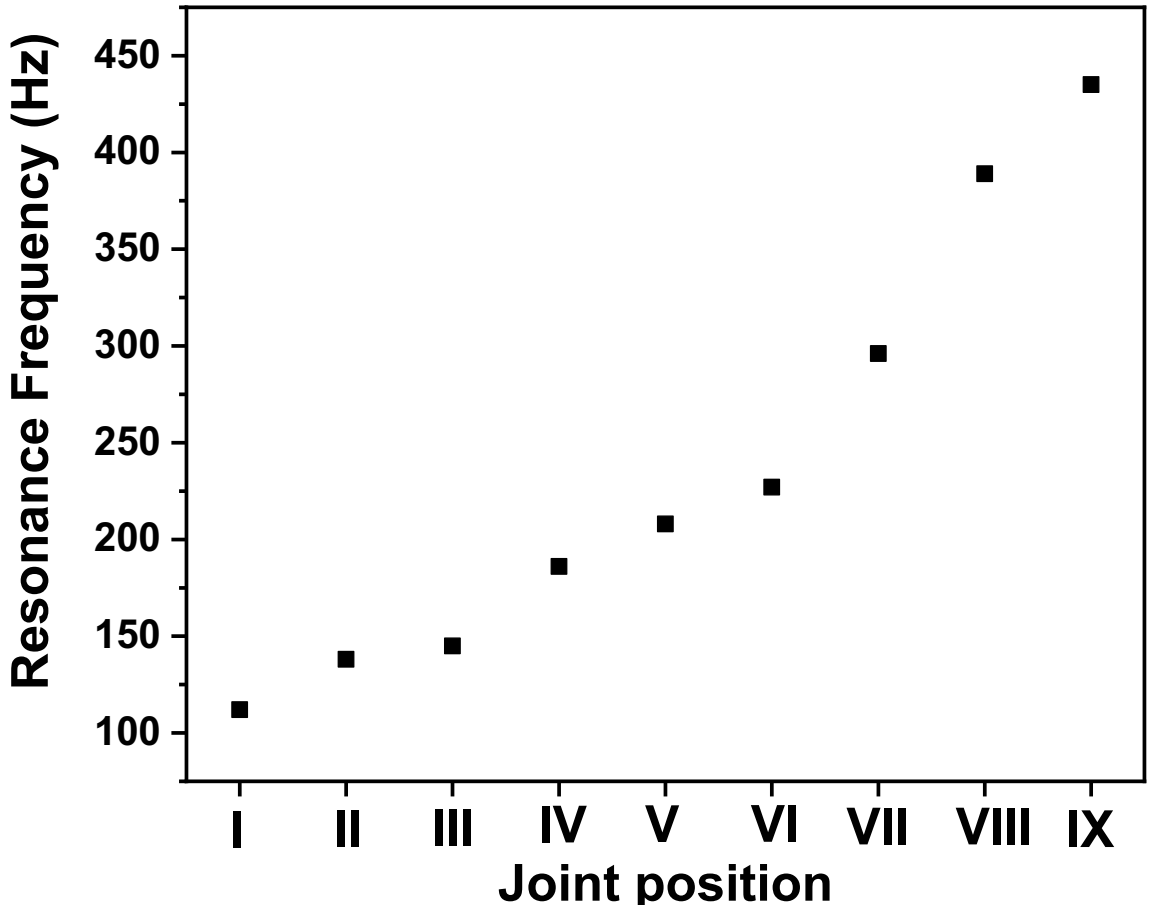

Fig. S13 The resonance frequency values for each single-joint antennae.

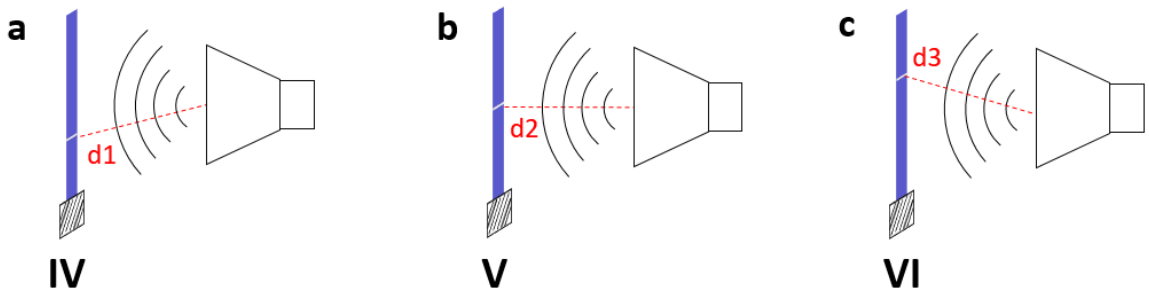

Fig. S14 Schematic illustration of the experimental set-up for testing different single-joint antennae. (a) Testing set-up for "IV". "d1" means the distance between speaker and the joint. (b) Testing set-up for "V". "d2" means the distance between speaker and the joint. (c) Testing set-up for "VI". "d3" means the distance between speaker and the joint. d2 is shorter than d1 and d3.

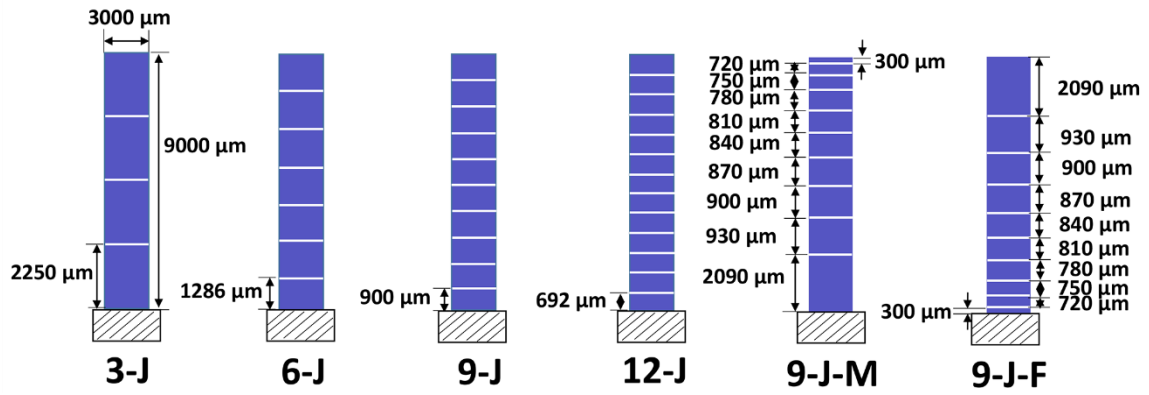

Fig. S15 Dimensions for multiple-joint antennae. 3-J, 6-J, 9-J, and 12-J have evenly-spaced joints. The joints of 9-J-M and 9-J-F are not evenly spaced. 9-J-M and 9-J-F mimic male and female mosquito antennae with gradually decreased[1] and increased spacing,[2] respectively.

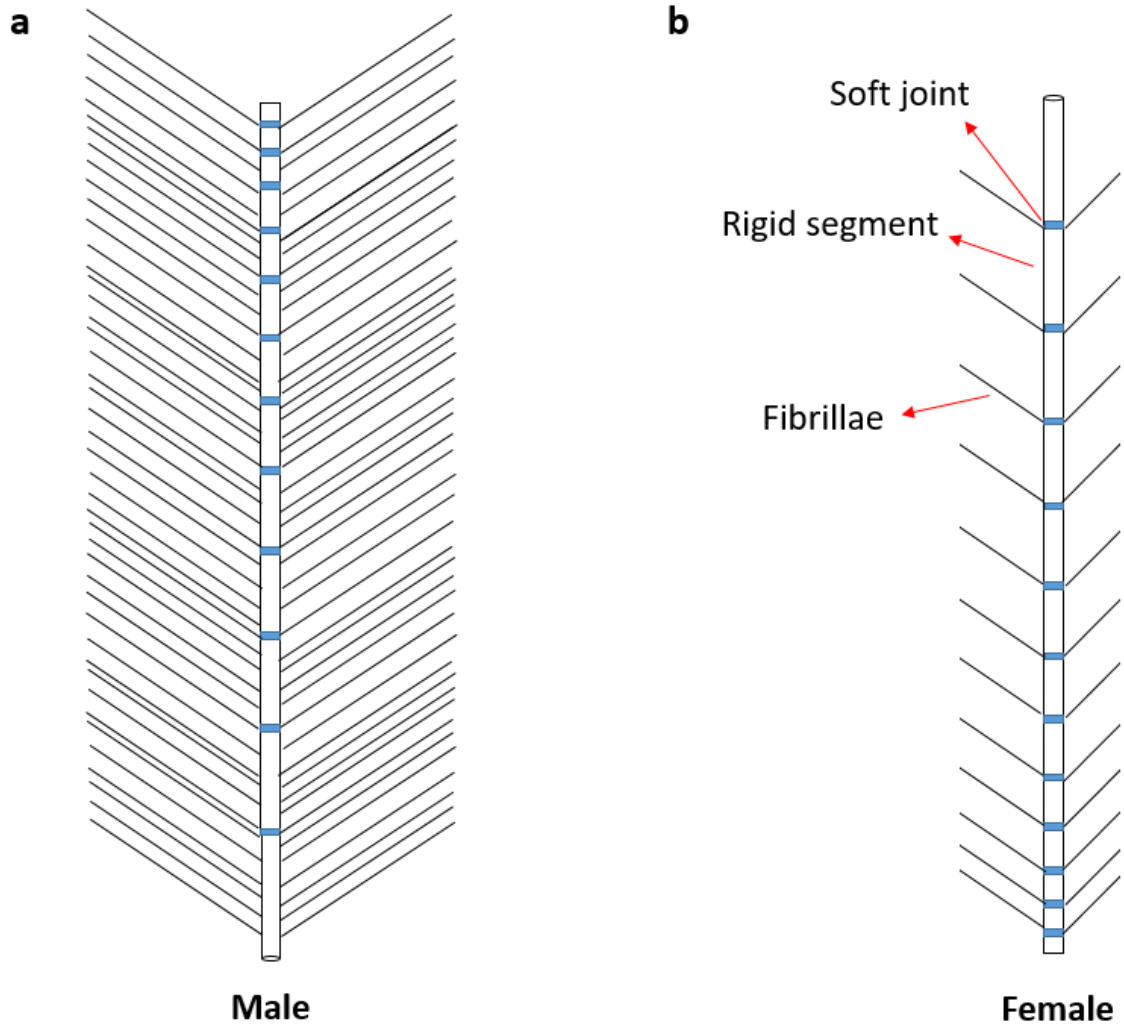

Fig. S16 (a) Schematic image of male antennae of *T. brevipalpis*. It has rigid segments and soft joints distributed along the antennae. The segment length continuously decrease from bottom fixed end to the top free end.[1] The fibrillae is very dense and long. (b) Schematic image of female antennae of *An. quadriannulatus*. It also has rigid segments and soft joints distributed along the antennae. The segment length continuously increase from bottom fixed end to the top free end.[2] The fibrillae density is low and its length is short.

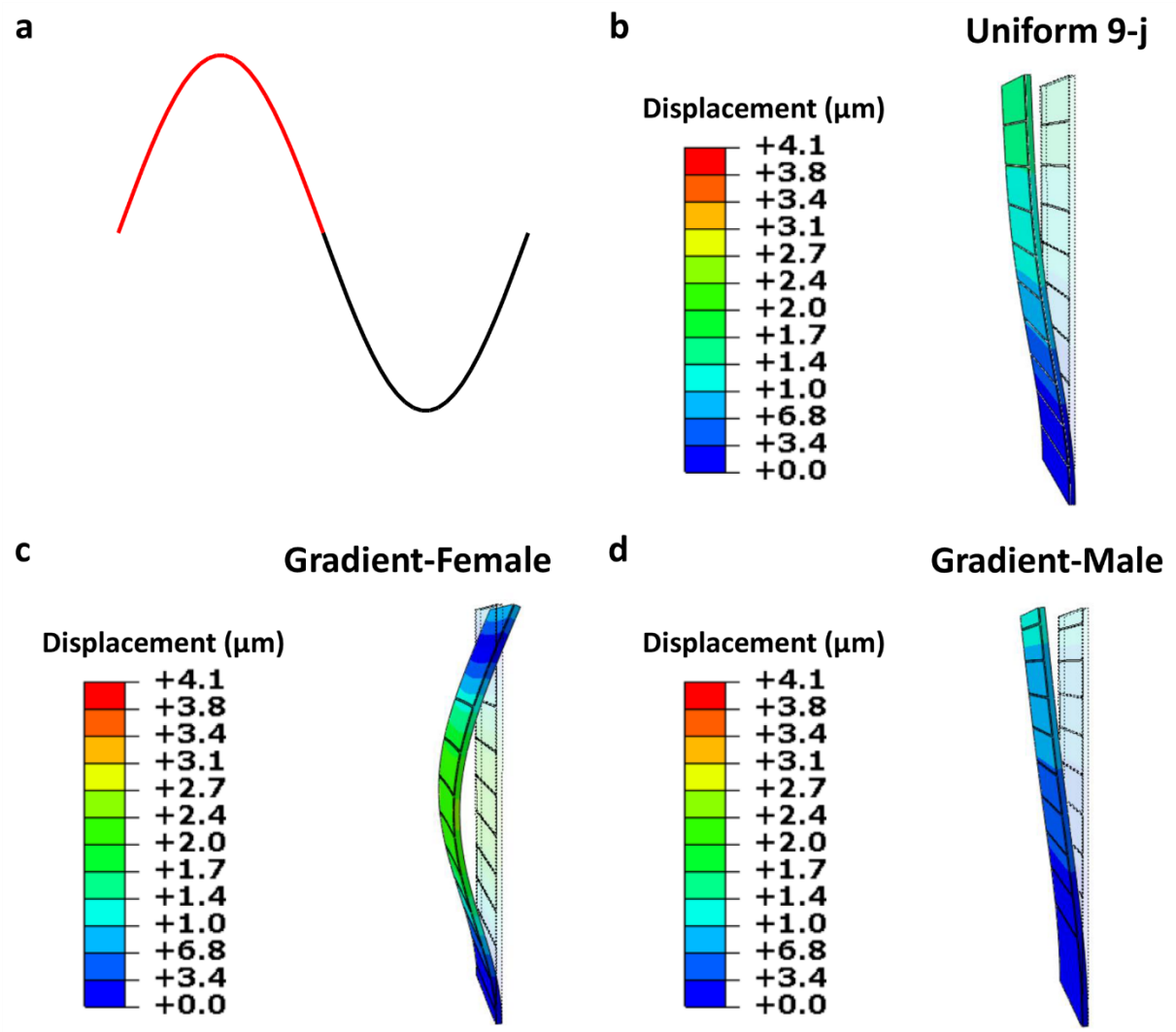

Fig. S17 (a) Simulated sound signals in the form of sine wave. The red color means the signal is in the positive half cycle. (b) The vibration state of 9-J antennae. (c) The vibration state of 9-J-F antennae. (d) The vibration state of 9-J-M antennae. Note that the transparent antennae image shown in each figure is the initial state of being still.

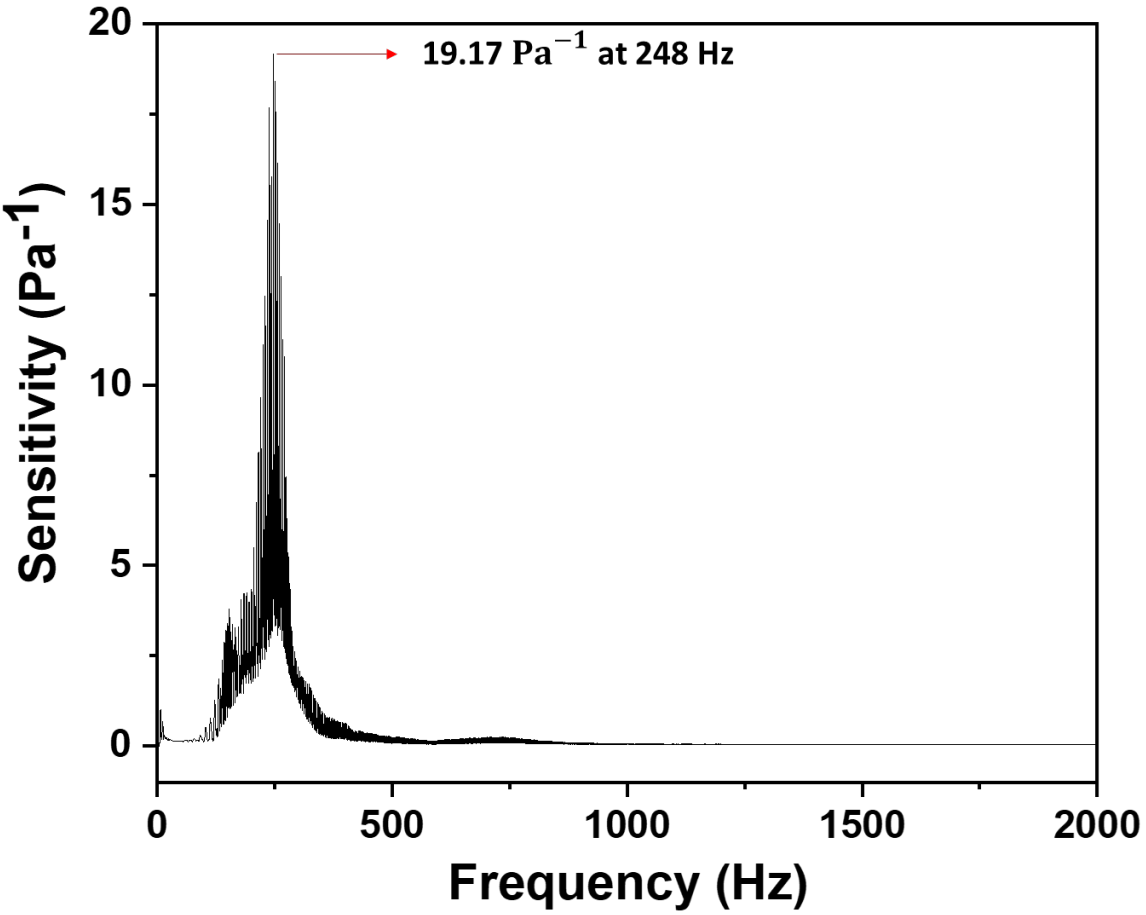

Fig. S18 Sensitivity for artificial female antennae (9-J-F) in the frequency range from 0 to 2000 Hz. The applied sound volume is 15%. The equation for calculating the sensitivity is[9]

$$S = \frac{\Delta R/R_0}{P} = \frac{(R - R_0)/R_0}{P_0 \times 10^{L_P/20}}$$

where R_0 and R are resistances of the antennae before and during sound broadcasting. P_0 is the reference sound pressure of 0.00002 Pa and L_P is the sound pressure level in decibel. The resonance frequency (RF) is the frequency when the sensitivity has maximum values. For the artificial female antennae, RF is 248 Hz.

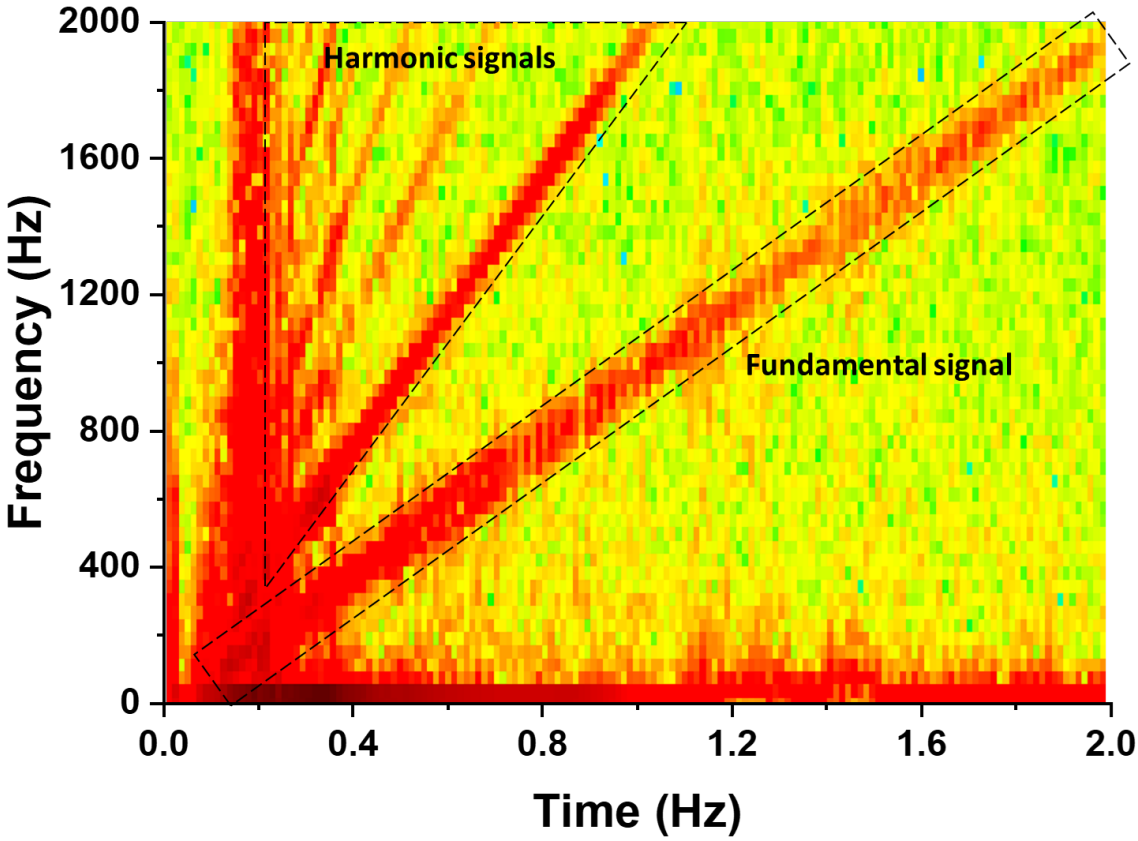

Fig. S19 STFT analysis of the artificial female antennae's response under a chirp signal (0–2000 Hz) for 2 s. The applied sound volume is 15%. As shown in the dashed rectangular frame, full range response is almost achieved. But the antennae could not recognize sound in the range of 0 - ~80 Hz because the SPL for this frequency range is too small (same as background noise's SPL). The red lines in the dashed triangle frame represents the harmonic signals.

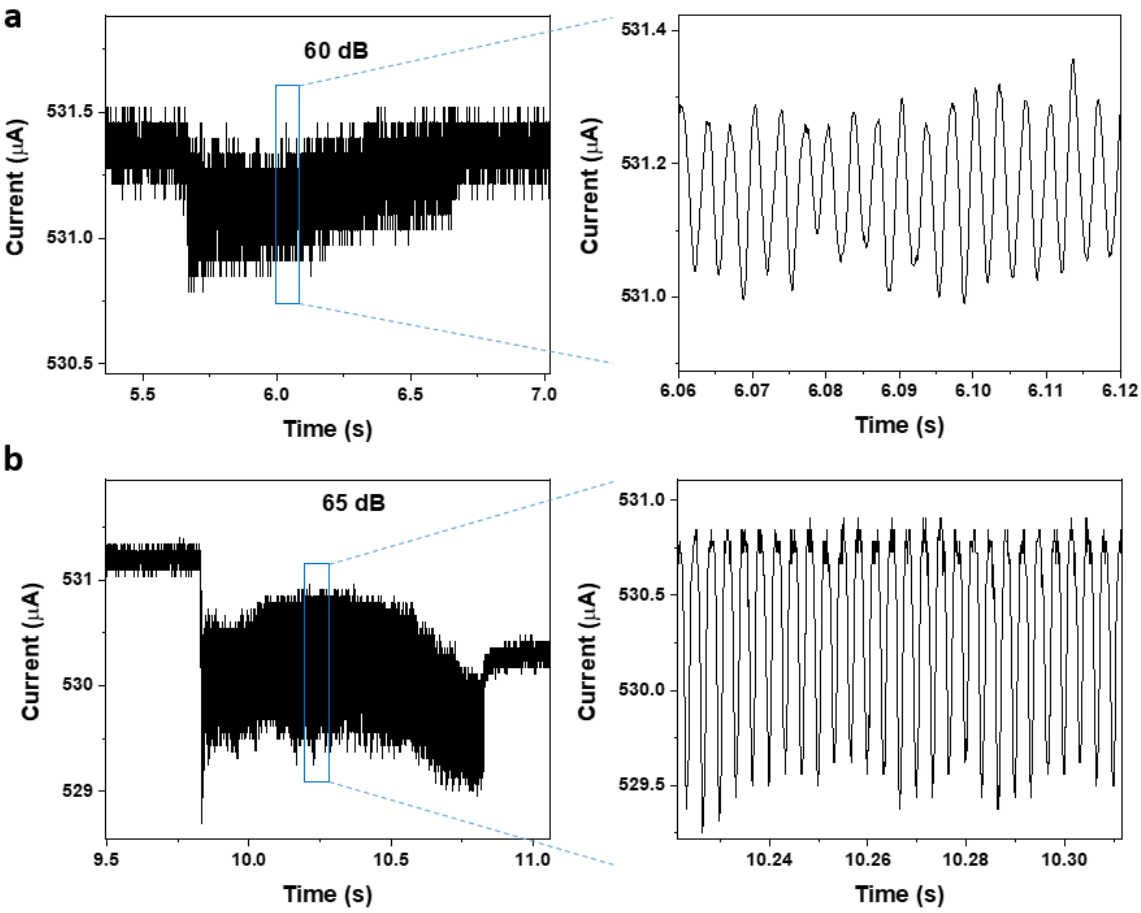

Fig. S20 We used 300 Hz sound for test. The sound pressure level (SPL) increased from 58.4 dB to 86.4 dB (0 - 42.8s). Enlarged view of antennae output current versus time under a SPL of (a) 60 dB and (b) 65 dB.

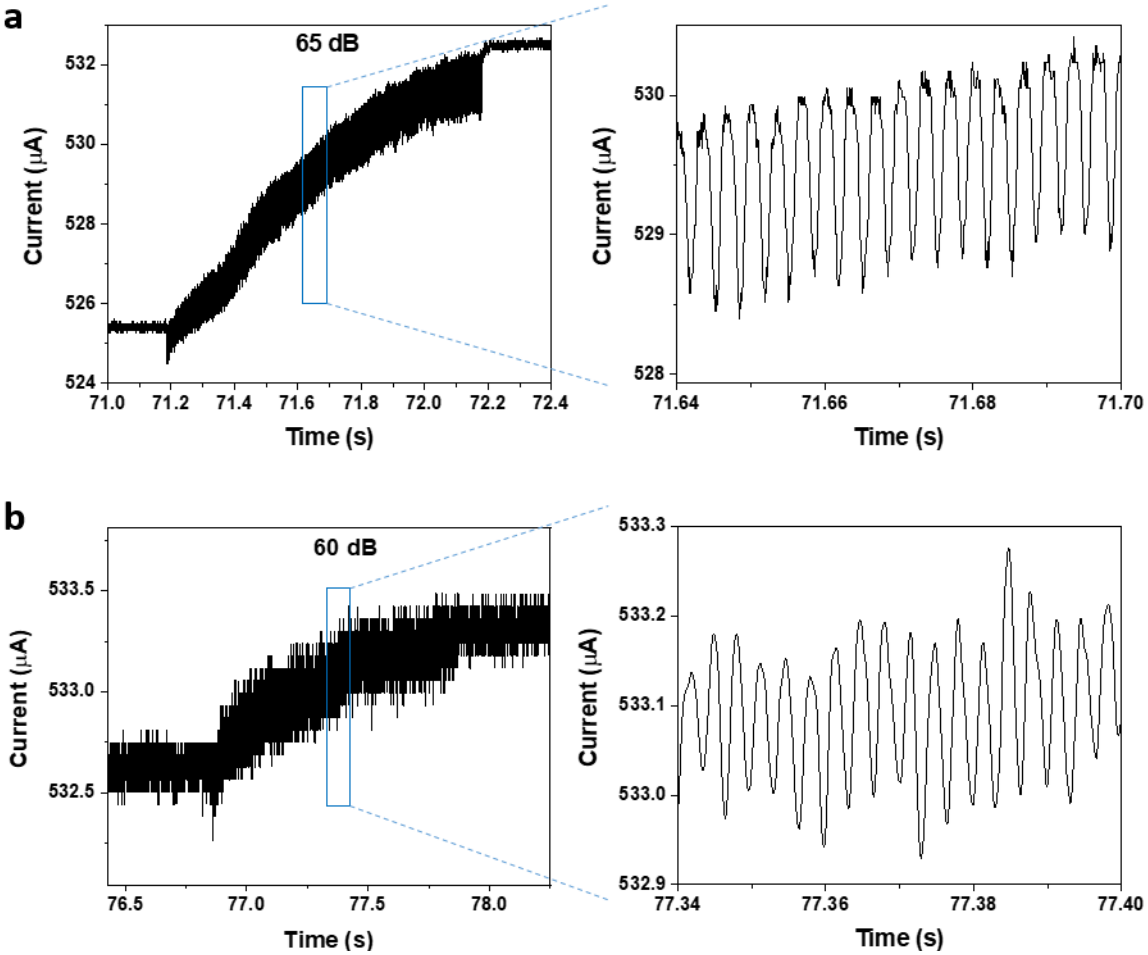

Fig. S21 We used 300 Hz sound for test. The sound pressure level decreased from 86.4 dB to 58.4 dB (42.8 - 83.9 s). Enlarged view of antennae output current versus time under a SPL of (a) 65 dB and (b) 60 dB.

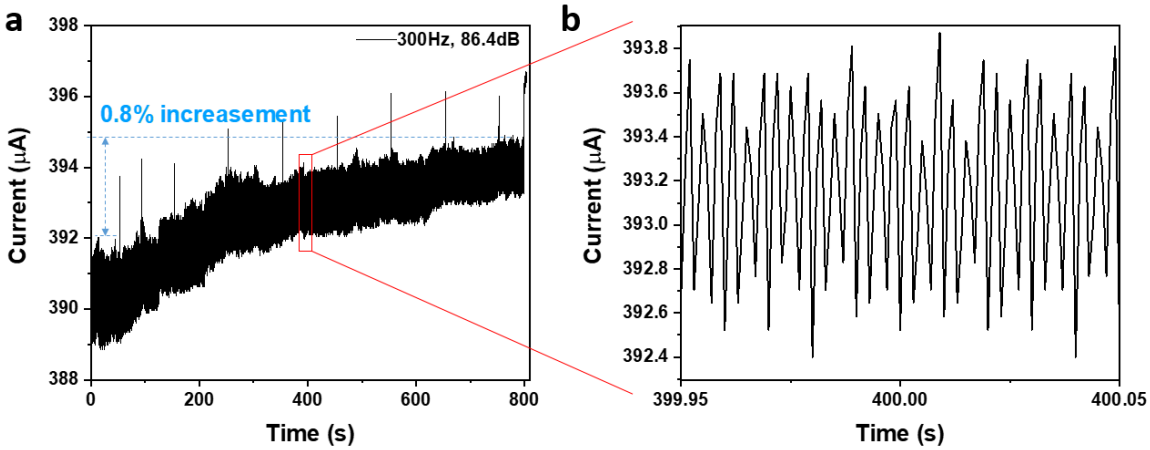

Fig. S22 Durability test for the artificial female mosquito antennae. The applied sound's frequency is 300 Hz. (a) Output current of the antennae under a sound pressure level of 86.4 dB. The sound lasted for 800 s. (b) Enlarged view of (a).

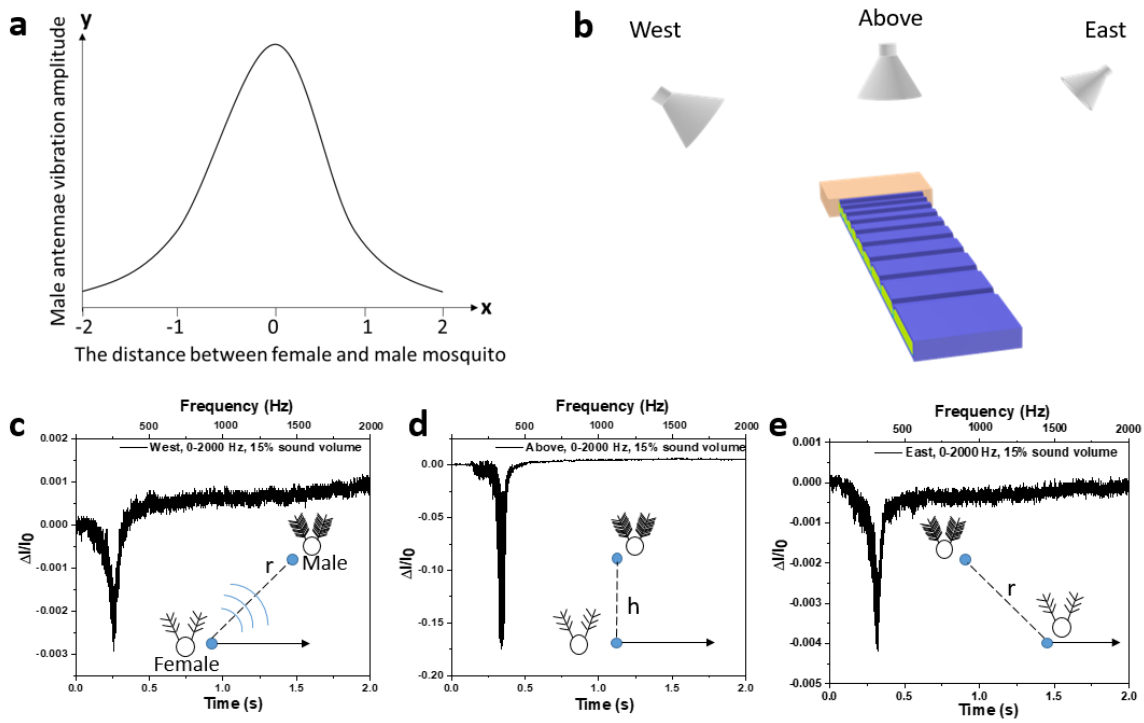

Fig. S23 (a) The relationship between male mosquito's antennae vibration amplitude and the distance between male and female mosquito.[3] (b) The experimental set-up for mimicking the scene that a female mosquito fly passing our antennae. At first we put the speaker at the west direction to the antennae (directions of speaker and antennae were kept at 45°). The distance between the speaker and antennae is ~7 mm; then we put the speaker above the antennae with a distance of 5 mm; finally we put the speaker at the east direction to the antennae (directions of speaker and antennae were kept at 45°) with a distance ~7 mm. The applied sound is a chirp signal (0–2000 Hz) for 2 s with 15% sound volume. (c-e) The antennae response during the experiments in (b).

Table S1. Comparison of the state-of-the-art soft acoustic sensors.

Structure	Sensor type	Sensitivity	Detected frequency range (Hz)	Detection limit (dB)	Response time (ms)	Ref.
Suspended beam	Triboelectric	1.74-13.1 mV Pa^{-1}	294.8 - 2311	70	~12	4
2D sheet	Resistive	0.00048 Pa^{-1}	N/A	65	~250	5
2D sheet	Resistive	> 0.00114 Pa^{-1}	N/A	N/A	< 17	6
Suspended membrane	Resistive	N/A	20-2000	83	0.5	7
Suspended membrane	Piezoelectric	N/A	100-1600	40	N/A	8
Suspended membrane	Resistive	0.48–4.26 Pa^{-1}	319-3000	70	N/A	9
3D Cavity	Triboelectric	9.54 V Pa^{-1}	10 -1700	70	N/A	10
Free-standing 1D antennae	**Resistive**	**19.17 Pa^{-1}**	**100-2000**	**58.4**	**1.14**	**this work**

References

1 B. D. Saltin, Y. Matsumura, A. Reid, J. F. Windmill, S. N. Gorb and J. C. Jackson, *J. R. Soc. Interface*, 2019, **16**, 20190049.

2 R. J. Pitts and L. J. Zwiebel, *Malar. J.*, 2006, **5**, 26.

3 J. C. Jackson and D. Robert, *Proc. Natl. Acad. Sci. U. S. A.*, 2006, **103**, 16734–16739.

4 J. Jang, J. W. Lee, J. H. Jang and H. Choi, *Adv. Healthc. Mater.*, 2016, **5**, 2481–2487.

5 L. W. Lo, H. Shi, H. Wan, Z. Xu, X. Tan and C. Wang, *Adv. Mater. Technol.*, 2020, **5**, 1900717.

6 S. Gong, W. Schwalb, Y. Wang, Y. Chen, Y. Tang, J. Si, B. Shirinzadeh and W. Cheng, *Nat. Commun.*, 2014, **5**, 3132.

7 Q. Zhang, C. Ji, L. Lv, D. Zhao, J. Ji, K. Zhuo, Z. Yuan, W. Zhang and S. Sang, *Soft Robot.*, 2021, **8**, 352–363.

8 H. S. Lee, J. Chung, G. T. Hwang, C. K. Jeong, Y. Jung, J. H. Kwak, H. Kang, M. Byun, W. D. Kim, S. Hur, S. H. Oh and K. J. Lee, *Adv. Funct. Mater.*, 2014, **24**, 6914–6921.

9 S. Gong, L. W. Yap, Y. Zhu, B. Zhu, Y. Wang, Y. Ling, Y. Zhao, T. An, Y. Lu and W. Cheng, *Adv. Funct. Mater.*, 2020, **30**, 1910717.

10 J. Yang, J. Chen, Y. Liu, W. Yang, Y. Su and Z. L. Wang, *ACS Nano*, 2014, **8**, 2649–2657.